Mean Streamline Aerodynamic Performance Analysis of Centrifugal Compressors

R. H. Aungier
Product Development,
Elliott Company,
Jeannette, PA 15644

Aerodynamic performance prediction models for centrifugal compressor impellers are presented. In combination with similar procedures for stationary components, previously published in the open literature, a comprehensive mean streamline performance analysis for centrifugal compressor stages is provided. The accuracy and versatility of the overall analysis is demonstrated for several centrifugal compressor stages of various types, including comparison with intrastage component performance data. Detailed validation of the analysis against experimental data has been accomplished for over a hundred stages, including stage flow coefficients from 0.009 to 0.15 and pressure ratios up to about 3.5. Its application to turbocharger stages includes pressure ratios up to 4.2, but with test uncertainty much greater than for the data used in the detailed validation studies.

Introduction

Mean streamline aerodynamic performance analysis continues to play a key roll in the design and application of centrifugal compressors. Despite impressive progress in computational fluid dynamics procedures, mean streamline methods continue to be the most accurate and the most practical method of predicting the performance of a stage or a component of a stage. Whitfield and Baines (1990) and Cumpsty (1989) contain good recent overviews of mean streamline methods. The analysis described here has been under development for over twenty years. Literally hundreds of different stages have been analyzed with it.

Detailed comparison of experimental data with predicted results has been accomplished for over a hundred stages. However, the best test of a performance analysis is its application to design activity. Weaknesses in the analysis are most clearly exposed when designers use it to guide them to better performing stages or components. This analysis has been revised and requalified each time sufficient test results from stage development programs were available to define significant deficiencies. The seventh major revision of the analysis is now in use. It has been successfully supporting stage development activity for over four years. It is applied to a variety of stage types, including process compressors, air compressors, and turbochargers. The detailed validation studies include stage flow coefficients, ϕ, from 0.009 to 0.15 and pressure ratios up to about 3.5. Good results have also been obtained on applications to turbocharger stages for pressure ratios up to about 3.5. Good results have also been obtained on applications to turbocharger stages for pressure ratios up to 4.2. However, test uncertainty for these units is much greater than for data used in the detailed validation studies.

Methods used in this analysis to predict performance for stationary components have previously been published in the open literature. These include prediction methods for vaned diffusers (Aungier, 1990), vaneless diffusers and return systems (Aungier, 1993), and volutes (Weber and Koronowski, 1986). The present paper provides a description of the impeller performance prediction methods to complete the description of the overall analysis. The overall centrifugal compressor stage performance analysis is compared to experiment for a series of stages of widely varying type.

The mean streamline performance analysis is a modular structured computer program. It has modules to analyze the various stage components as they appear in the stage. Figure 1 illustrates a general return channel style stage with the key computing stations numbered 1 through 7. The analysis provides detailed mean streamline fluid dynamic and performance data at each numbered station. Figures 2 and 3 illustrate some of the more important impeller geometric parameters.

Impeller Work Input

The general form of the impeller work input equation is

$$(\mu/\eta) = \Delta H/U_2^2 = I_B + I_{DF} + I_L + I_R \qquad (1)$$

where the terms on the right-hand side are (in order) the contributions due to the blades, windage and disk friction, seal leakage, and recirculation. The blade work input is given by

$$I_B = \sigma(1 - \lambda\phi_2 \cot \beta_2) - U_1 C_{u1}/U_2^2 \qquad (2)$$

The last term in Eq. (2) accounts for prewhirl effects. The term in parentheses can be recognized as the ideal (perfect blade guidance) dimensionless tip tangential velocity, $C_{u2\ \text{ideal}}$. The slip factor formulation of Wiesner (1967) is used

$$\sigma = 1 - \frac{\sin \alpha_{c2}\sqrt{\sin \beta_2}}{z^{0.7}} \qquad (3)$$

which holds up to the limiting radius ratio given by

$$\epsilon_{\text{LIM}} = \frac{\sigma - \sigma_*}{1 - \sigma_*}$$

$$\sigma_* = (19 \text{ deg} + 0.2\beta_2) \qquad (4)$$

When the actual radius ratio exceeds the limiting value, a corrected slip factor is computed by

$$\sigma_{\text{COR}} = \sigma\left[1 - \left(\frac{\epsilon - \epsilon_{\text{LIM}}}{1 - \epsilon_{\text{LIM}}}\right)^{\sqrt{\beta_2/10}}\right] \qquad (5)$$

When splitter blades are present, the effect of the limiting radius ratio is checked independently for full and splitter blades. Hence, extremely short splitter blades will be recognized as ineffective in contributing to the impeller work input.

Contributed by the International Gas Turbine Institute and presented at the ASME–NJIT–HI–STLE Rotating Machinery Conference and Exposition (ROCON'93), Somerset, New Jersey, November 10–12, 1993. Manuscript received at ASME Headquarters July 1994. Associate Technical Editor: N. A. Cumpsty.

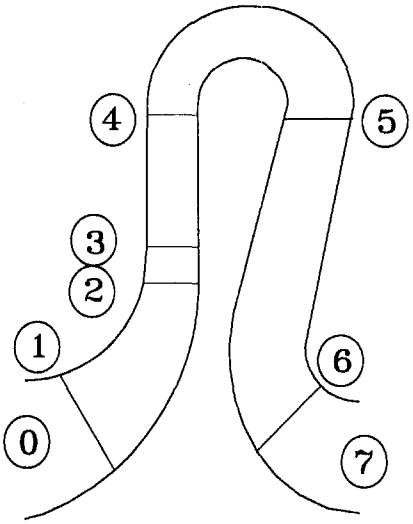

Fig. 1 Stage computing stations

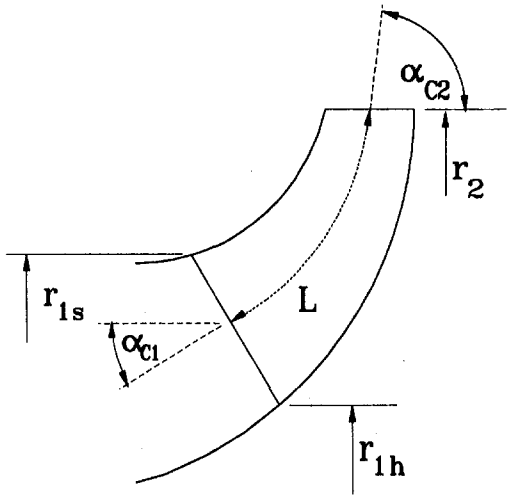

Fig. 2 Impeller Gaspath geometry

The impeller distortion factor, λ, is related to the tip aerodynamic blockage, B_2, by

$$\lambda = 1/(1 - B_2) \tag{6}$$

The equation used to predict the impeller tip blockage is

$$B_2 = (\Delta q_{SF} + \Delta q_{HS}) \frac{U_2^2}{W_2^2} + \left[0.3 + \frac{b_2^2}{L_B^2}\right] \frac{A_R^2 v_1 b_2}{v_2 L_B} + \frac{s_{CL}}{2b_2} \tag{7}$$

where the first term on the right-hand side contains skin friction and hub-to-shroud distortion loss coefficients to be presented later. The area ratio, A_R, is given by

$$A_R = A_2 \sin \beta_2 / (A_1 \sin \beta_{th}) \tag{8}$$

where β_{th} is suction surface blade angle at the impeller throat. A_R is similar to the ratio of the discharge area to the throat area. Throat area was not used directly because users of the analysis occasionally have chosen to adjust the input throat area to match an experimental choke limit. To avoid false variations in work input when this is done, the form given above was used to develop the empirical correlation. An equally accurate correlation could be developed using the throat area, but the present

Nomenclature

A = an area inside the blade passage
a = sound speed
B = fractional area blockage
b = hub-to-shroud passage width
C = absolute velocity
C_M = disk torque coefficient
C_m = absolute meridional velocity
C_r = throat contraction ratio, Eq. (20)
C_u = absolute tangential velocity
c_f = skin friction coefficient
D_{eq} = equivalent diffusion factor, Eq. (11)
d = diameter
d_h = hydraulic diameter
f_c = head loss correction factor, Eq. (31)
H = total enthalpy
h = static enthalpy
h_{th} = blade-to-blade throat width
I = work input coefficients, Eq. (1)
K = clearance gap swirl parameter = $C_u/(\omega r)$
L = blade mean streamline meridional length = $m_2 - m_1$
L_{SB} = splitter blade mean streamline meridional length
L_B = length of blade mean camberline
M = Mach number
M_u = rotational Mach number = U_2/a_{0T}
m = meridional coordinate
$\dot{m}$ = mass flow
P = pressure
R = rothalpy, Eq. (29)
r = radius
S = entropy
s = clearance gap width
U = blade speed = ωr; leakage tangential velocity
v = gas specific volume
W = relative velocity
W_u = relative tangential velocity
z = effective number of blades = $z_{FB} + z_{SB} L_{SB}/L$
z_{FB} = number of full-length blades
z_{SB} = number of splitter blades
α = flow angle with respect to tangent
α_c = streamline slope angle with axis
β = blade angle with respect to tangent
Δq = adiabatic head loss coefficient = $\Delta H/U_2^2$
ϵ = impeller meanline radius ratio = r_1/r_2
η = adiabatic efficiency
κ = streamline curvature, Eq. (15)
λ = tip distortion factor, Eq. (6)
μ = adiabatic head coefficient and gas viscosity
ξ = distance along blade mean camberline
ρ = gas density
σ = slip factor = $C_{u2}/C_{u2\ ideal}$
ϕ = stage flow coefficient = $\dot{m}/(\pi \rho_{T0} r_2^2 U_2)$
ϕ_2 = tip flow coefficient = C_{m2}/U_2
ω = rotation speed

Subscripts

B = a blade parameter
C = cover parameter
CL = clearance gap parameter
D = disk parameter
DF = disk friction parameter
h = parameter on the hub contour
L = leakage parameter
p = blade pressure surface parameter
R = recirculation parameter
s = shroud contour or blade suction surface parameter
T = total thermodynamic condition
th = throat parameter
0 = impeller eye condition
1 = impeller blade leading edge condition
2 = impeller tip condition
4 = diffuser exit condition
7 = stage exit condition

Superscripts

* = sonic flow condition
′ = value relative to rotating frame of reference

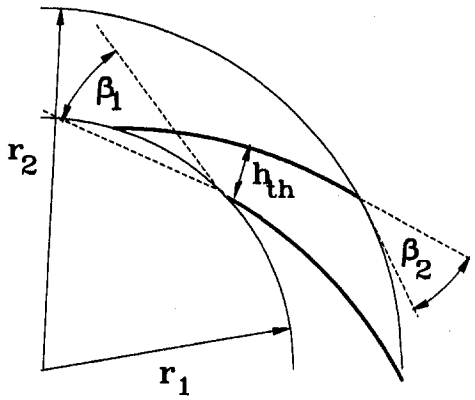

Fig. 3 Impeller blade geometry

model uses the form in Eq. (8). Equation (7) is the product of many years of development, directed to work input prediction for over a hundred different impellers. It is deceptively simple, but it is very effective in modeling the complex distortion effect for a broad range of impeller types. It seeks to model a number of different mechanisms, such as skin friction, hub-to-shroud flow distortion, volume ratio, flow diffusion, clearance (for open impellers) and blade aspect ratio. These various mechanisms assume vastly different significance for different impeller types. For example, dominant terms for low-specific-speed impellers are negligible for high-specific-speed impellers, and inversely.

Impeller windage and disk friction and cover seal leakage work input for covered impellers are given by

$$I_{DF} + I_L = \frac{(C_{MD} + C_{MC})\rho_2 U_2 r_2^2}{2\dot{m}} + \frac{\dot{m}_L I_B}{\dot{m}} \tag{9}$$

For open impellers, they are given by

$$I_{DF} + I_L = \frac{C_{MD}\rho_2 U_2 r_2^2}{2\dot{m}} + \frac{\dot{m}_{CL} U_{CL}}{2\dot{m} U_2} \tag{10}$$

which assumes half of the clearance gap leakage flow is re-entrained into the blade passage flow and re-energized by the impeller. The appendix describes the calculation of the torque coefficients and leakage parameters in Eqs. (9) and (10).

Impeller tip flow recirculation is observed to contribute to the impeller work input for some impellers, particularly high head coefficient impellers with excessive blade loading levels and at low tip relative flow angles. Impeller blade loading levels are evaluated with a generalization of the equivalent diffusion factor, D_{eq}, of Lieblein (1959) given by

$$W_{\max} = (W_1 + W_2 + \Delta W)/2$$

$$D_{eq} = W_{\max}/W_2 \tag{11}$$

where the average blade velocity difference, ΔW, is computed from standard irrotational flow relations, assuming an ideal or optimum blade loading style.

$$\int_0^{L_B} (W_s - W_p)d\xi = 2\pi(r_2 C_{U2} - r_1 C_{U1})/z$$

$$W_s - W_p = \Delta W[1 - |2\xi/L_b - 1|]$$

$$\Delta W = 2\pi d_2 U_2 I_B/(zL_B) \tag{12}$$

The blade stall limit of Lieblein ($D_{eq} = 2$) has been found to be appropriate for impellers also. Hence, when $D_{eq} > 2$, the recirculation work input coefficient is computed from

$$I_R = (D_{eq}/2 - 1)[W_{u2}/C_{m2} - 2\cot\beta_2]$$

$$I_R \geq 0 \tag{13}$$

Impeller Internal Losses

The adiabatic head loss coefficient in the inlet passage (stations 0 to 1) can be computed with the vaneless passage performance analysis of Aungier (1993). A simple approximation to that analysis has also been found to be sufficient for this purpose.

$$\Delta q_0 = \frac{C_{m1}^2}{2U_2^2}\left[\frac{2c_f(m_1 - m_0)}{b_1} + \frac{\alpha_{c1} - \alpha_{c2}}{13}\right] \tag{14}$$

Equation (14) approximates the friction and curvature loss models of the more exact analysis. The skin friction coefficient is computed from an empirical correlation of pipe friction factors for laminar, transitional and turbulent flow, including surface roughness effects (e.g., see Schlichting, 1979).

Entrance losses are computed for the hub, shroud, and mean streamline positions. The mean streamline entrance velocity is computed from the specified inlet prewhirl, C_{u1}, and conservation of mass. The hub and shroud entrance meridional velocities are estimated from the inlet streamline curvature, κ_1,

$$\kappa = \frac{\partial \alpha_c}{\partial m}$$

$$C_{mh1} = C_{m1}[1 - \kappa_1 b_1/2]$$

$$C_{ms1} = C_{m1}[1 + \kappa_1 b_1/2] \tag{15}$$

If any of the three entrance relative velocities exceeds sonic conditions, normal shock wave relations are used to reduce it to a subsonic value and compute a shock loss, Δq_{sh}. Fundamental shock wave mass and momentum conservation relations are used for this purpose to permit analysis of nonideal gas mixtures. The incidence loss is computed by

$$\Delta q_{\text{inc}} = 0.4(W_1 - C_{m1}/\sin\beta_1)^2/U_2^2 \tag{16}$$

Equation (16) is applied at the hub, shroud, and mean surfaces. The overall incidence and shock losses are then combined in a weighted average, with the mean streamline values weighted 10 times as heavy as the hub and shroud values. At positive incidence angles, Eq. (16) occasionally underestimates the entrance loss. For some impellers, the flow adjustment between the leading edge and the throat is the more significant effect. An entrance diffusion loss is computed to account for these situations:

$$\Delta q_{\text{DIF}} = 0.4(W_1 - W_{th})^2/U_2^2 - \Delta q_{\text{inc}}$$

$$\Delta q_{\text{DIF}} \geq 0 \tag{17}$$

The flow diffusion from the blade inlet to the throat has been found to be a primary indicator of inducer stall. The specific stall criterion derived from available test data is

$$W_{1s}/W_{th} > 1.75 \tag{18}$$

Kosuge et al. (1982) have used the same parameter to correlate the onset of impeller rotating stall as a function of throat Mach number. When inducer stall is predicted, the diffusion loss is limited by

$$\Delta q_{\text{DIF}} \geq 0.5(W_{1s} - 1.75W_{th})^2/U_2^2 - \Delta q_{\text{inc}} \tag{19}$$

Aerodynamic blockage in the throat is modeled by a contraction ratio computed from

$$C_r = \sqrt{A_1 \sin\beta_1/A_{th}}$$

$$C_r \leq 1 - (A_1 \sin\beta_1/A_{th} - 1)^2 \tag{20}$$

The contracted throat area and the sonic flow throat area, A^*_{th}, are used to compute a choking loss:

$$x = 10(1.1 - A^*_{th}/(C_r A_{th})$$

$$\Delta q_{CH} = 0; \quad x \le 0$$

$$\Delta q_{CH} = (W_1/U_2)^2(0.05x + x^7)/2; \quad x > 0 \qquad (21)$$

The friction factor correlation mentioned earlier is used to compute the impeller friction loss using a hydraulic diameter, d_H, that is the average of the throat and discharge values.

$$\Delta q_{SF} = 2c_f(\bar{W}/U_2)^2 L_B/d_H$$

$$\bar{W}^2 = (W_1^2 + W_2^2)/2$$

$$\bar{W}^2 \ge (W_{th}^2 + W_2^2)/2 \qquad (22)$$

Blade loading and hub-to-shroud loading losses are computed as mixing losses derived from the integrated difference between the average and mass-averaged relative velocity squared for the distorted profiles. The relations used are

$$\Delta q_{BL} = (\Delta W/U_2)^2/48$$

$$\Delta q_{HS} = (\bar{\kappa}\bar{b}\bar{W}/U_2)^2/12$$

$$\bar{\kappa} = (\alpha_{c2} - \alpha_{c1})/L$$

$$\bar{b} = (b_1 + b_2)/2$$

$$\bar{W} = (W_1 + W_2)/2 \qquad (23)$$

where ΔW is given in Eq. (12). Similarly, a discharge profile distortion loss is computed from

$$\Delta q_\lambda = 0.5(\lambda - 1)^2\phi_2^2 \qquad (24)$$

For open impellers, the clearance loss is given by

$$\Delta q_{CL} = \frac{\dot{m}_{CL}\Delta P_{CL}}{\dot{m}\rho U_2^2} \qquad (25)$$

where the calculation of the clearance gap leakage parameters is described in the appendix. A wake mixing loss is computed, assuming that the wake contains stagnant fluid, which mixes with free stream fluid with velocity W_{SEP}. Separation is assumed to occur inside the blade passage if $D_{eq} > 2$. The loss is given by

$$\Delta q_{MIX} = 0.5[(W_{SEP} - W_{OUT})/U_2]^2$$

$$W_{SEP} = W_2; \quad D_{eq} \le 2$$

$$W_{SEP} = W_2 D_{eq}/2; \quad D_{eq} > 2$$

$$W_{OUT}^2 = [C_{m2}A_2/(\pi d_2 b_2)]^2 + W_u^2 \qquad (26)$$

where A_2 is the discharge area inside the blades. Using relative total thermodynamic conditions at the blade midpassage, the local value of sonic velocity is computed. From the maximum blade surface velocity from Eq. (11), the inlet critical Mach number (corresponding to locally sonic flow on the blade surfaces) is given by

$$M'_{cr} = M'_1 W^*/W_{max} \qquad (27)$$

If the inlet relative Mach number exceeds this critical Mach number, a supercritical Mach number loss is computed by

$$\Delta q_{cr} = 0.2[(M'_1 - M'_{cr})W_{max}/U_2]^2 \qquad (28)$$

Thermodynamic and Compressibility Effects

The analysis employs a general thermodynamic model suitable for one of several alternate nonideal gas equations of state (e.g., Aungier, 1994). The adjustment of total thermodynamic conditions relative to the rotating frame of reference is accomplished with the usual rothalpy parameter, R, which is constant along a stream surface:

$$R = H - UC_u \qquad (29)$$

R can be evaluated at the impeller inlet from the specified operating conditions. The conversion between R and the various total and static enthalpy values required is governed by

$$H' = h + W^2/2 = R + U^2/2$$

$$H = h + C^2/2 = R + UC_u \qquad (30)$$

These relations and isentropic state change logic offered by the various equations of state permit fluid dynamic calculations at the various locations in the impeller passage.

Largely due to historical reasons, the impeller loss models have been developed as adiabatic head (enthalpy) losses. This is strictly valid for incompressible flow, only. Since adiabatic head is not a state point parameter, a given head loss will produce different results when imposed at different locations. In this analysis, the losses occur in the blade passage, but are imposed at the impeller tip. Similarly, the loss formulations are based on relevant velocity heads, rather than the more correct velocity pressure, $P_t - P$. Again, this is strictly correct only for incompressible flow. The consequence of these two factors is a deterioration in prediction accuracy as rotational Mach number (or pressure ratio) increases.

The adiabatic head loss formulation imposes an enthalpy loss at constant entropy to predict the stage discharge total pressure. The correct approach is to impose an entropy rise at constant total enthalpy. From the basic thermodynamic relation,

$$TdS = dH - vdP \qquad (31)$$

it can be seen that a constant $\Delta q/T'_T$ provides the equivalent of a constant entropy rise. Consequently, the weaknesses of the head loss formulation are correctable by a head loss multiplying factor, f_c, given by

$$f_c = \frac{2T'_{T2}}{T'_{T1} + T'_{T2}} \frac{2(P'_{T1} - P_1)}{\rho_1 W_1^2} \qquad (32)$$

Then, the adiabatic head coefficient is given by

$$\mu_{2T} = I_B - f_c \Sigma \Delta q \qquad (33)$$

where the summation applies to the various loss coefficients presented in this paper. With this head loss correction procedure, the analysis has been used for stage pressure ratios up to 3.5 with no observable difference in prediction accuracy for different pressure ratios. Without this procedure, the deterioration of prediction accuracy with pressure ratio was quite noticeable.

Solution Procedure

The analysis of the impeller is conducted by an iterative solution to converge on the impeller tip mass flow. The impeller work input, losses and seal leakage are computed for each iteration. For covered impellers, the impeller mass flow is corrected

Table 1 Compressor stage data

STAGE	ϕ_{DES}	M_u	DISCHARGE	DIFFUSER
A	0.0093	0.50	RETURN CHANNEL	VANELESS
B	0.0525	0.70	RETURN CHANNEL	VANED
C	0.0950	1.38	VOLUTE	VANELESS
D	0.0950	1.38	VOLUTE	VANED
E	0.0860	0.70	RETURN CHANNEL	VANELESS
F	0.1250	0.70	RETURN CHANNEL	VANELESS

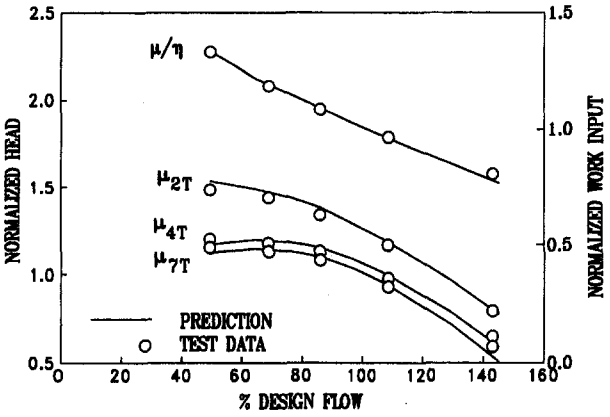

Fig. 4 Performance of Compressor A

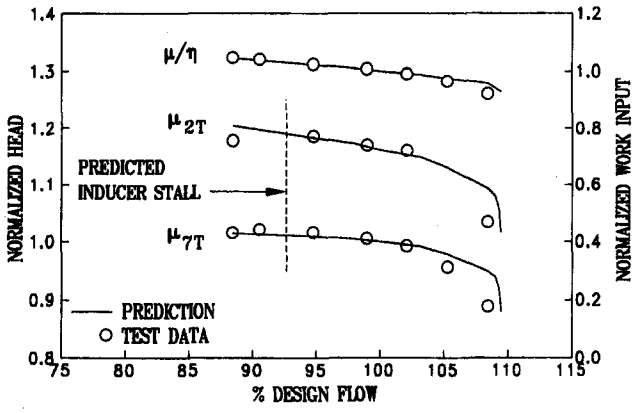

Fig. 6 Performance of Compressor C

to include the cover seal leakage flow. The total work input and tip adiabatic head coefficients define the tip thermodynamic conditions. The computed tip mass flow, $(\rho C_m A)_2$, is compared to the actual impeller mass flow and C_{m2} is updated until the process converges. Once convergence is achieved, the diffuser entrance mass flow is computed by adjusting the impeller mass flow for the seal leakage flows.

Results

The overall centrifugal compressor performance analysis is applicable to a broad range of stage types and operating conditions. Table 1 lists the particular stages for which predictions and test performance are compared in this paper. This performance analysis does not permit any "user adjustments" to the performance models. Hence, the results show predictions directly from the reported models for the precise stage geometry. With the exception of compressor A, these stages have been selected due to their very limited role in the development of the performance models used. The high quality of the test data and ultralow flow coefficient of Compressor A has made it a very valuable test of models relating to friction losses, windage and disk friction, and seal leakage for many years. Compressors B and D were used in the development of the vaned diffuser performance analysis (Aungier, 1990). Compressors C, D, and E were used to validate the head loss correction, Eq. (32), over the wide range of speeds for which they were tested. Compressor F was not used in the development of this analysis.

Figure 4 shows a comparison of predictions and test data for the ultralow flow coefficient compressor A. This stage experiences unusually high parasitic work (cover leakage, windage, and disk friction). The analysis does an excellent job of predicting both work and head, including impeller and diffuser exit heads.

Figure 5 compares predictions with test data for a medium-low flow coefficient vaned diffuser stage. This stage showed a pronounced stall on test with unstable operation at all flows lower than the peak head flow. The onset of this "stall" almost exactly corresponds to the predicted vaned diffuser stall. Tests on this stage with a vaneless diffuser confirm that the vaned diffuser is the source of this unstable operation.

Figure 6 compares predictions with test data for compressor C, a moderately high flow coefficient air compressor stage. This is a volute-type stage with a stage pressure ratio of 3.4, tested with a vaneless diffuser. Figure 7 shows results for the same compressor stage, but with a vaned diffuser. Clearly, the analysis models both stage configurations very well. Again, predicted vaned diffuser stall is shown on Fig. 7, which is almost exactly at the stage test surge flow. For the vaneless diffuser version, inducer stall is predicted in the test operating range. While the impeller tip head coefficient curve suggests a possible impeller stall in this region, intrastage component data for volute stages are rather unreliable due to the circumferential distortion imposed upon the stage by the volute.

Figure 8 shows results for compressor E, a medium flow coefficient return channel stage. It can be seen that agreement between predictions and test data is quite good, including the intrastage component discharge head coefficient curves.

Figure 9 shows results for the very high flow coefficient compressor stage F. This comparison is particularly significant since it is a recent design never used in the development of the analysis. Indeed, Fig. 9 is the projected performance provided by this analysis with actual test performance added. It can be seen that the analysis is quite accurate in its prediction of overall

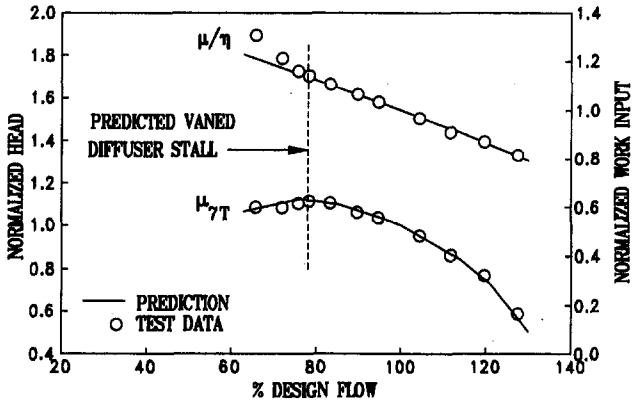

Fig. 5 Performance of Compressor B

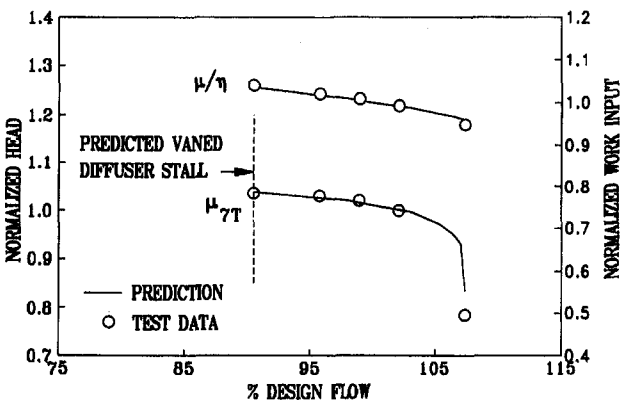

Fig. 7 Performance of Compressor D

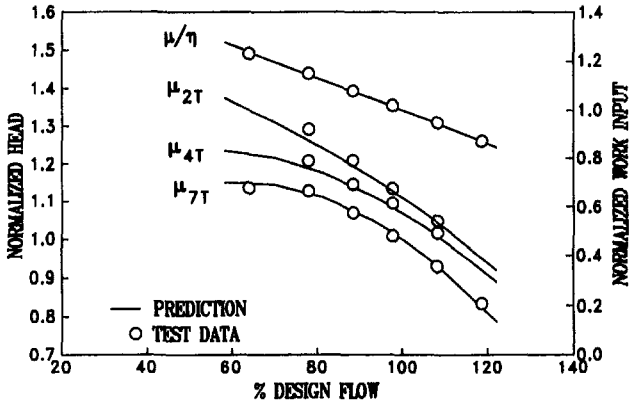

Fig. 8 Performance of Compressor E

and internal component performance. Note that the predicted inducer stall is quite close to the apparent impeller stall indicated by the impeller tip head curve. Further confirmation was obtained in a subsequent test where the vaneless diffuser width was significantly reduced, with no change in the surge flow. That strongly suggests that the impeller, rather than the diffuser, is the component governing surge.

Many additional detailed comparisons of test data with performance predictions from this analysis can be found in Aungier (1990, 1993), where the accuracy of the vaned diffuser, vaneless diffuser, and return system performance analyses is demonstrated.

Conclusions

The impeller analysis presented here, together with the stationary component analyses in the cited open literature, provide a comprehensive mean streamline aerodynamic performance prediction procedure for centrifugal compressor stages. This analysis has been qualified against experimental test data for over one hundred different stages, of widely varying types. Its prediction accuracy is generally excellent for any reasonably well-designed stage. On some very old designs (considered poorly designed by modern standards) the analysis can be less accurate. However, even then, it correctly identifies the weaknesses in those designs and it correctly predicts their performance to be poor. The minimal geometric data needed to apply these performance models is simply not sufficient to identify poor detailed design practice.

Detailed validation of the analysis against experiment has included stage flow coefficients from 0.009 to 0.15 and pressure ratios up to about 3.5. Good results have also been obtained for turbocharger stages at pressure ratios up to 4.2, but test data uncertainty for these units is much greater than for the data used in the detailed validation studies. Application of this analysis significantly beyond this range of experience would require additional validation studies.

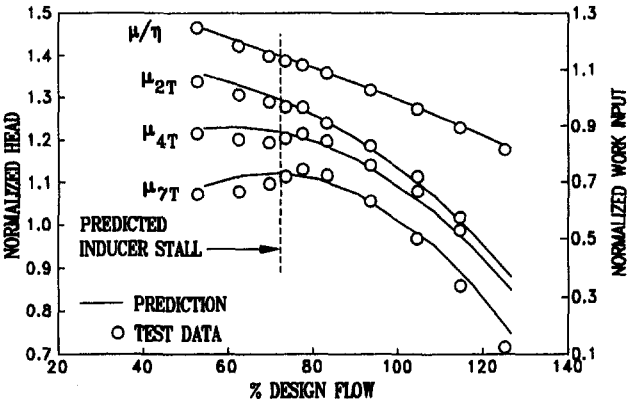

Fig. 9 Performance of Compressor F

References

Aungier, R. H., 1990, "Aerodynamic Performance Analysis of Vaned Diffusers," *Fluid Machinery Components,* ASME FED-Vol. 101, pp. 27–44.

Aungier, R. H., 1993, "Aerodynamic Design and Analysis of Vaneless Diffusers and Return Channels," ASME Paper No. 93-GT-101.

Aungier, R. H., 1994, "A Fast, Accurate Real Gas Equation of State for Fluid Dynamic Analysis Applications," *Contributed Papers in Fluids Engineering 1994,* ASME FED-Vol. 182, pp. 1–6; to be published in ASME *Journal of Fluids Engineering.*

Cumpsty, N. A., 1989, *Compressor Aerodynamics,* Longman Scientific and Technical, Essex, United Kingdom.

Daily, J. W., and Nece, R. E., 1960a, "Chamber Dimension Effects on Induced Flow and Frictional Resistance of Enclosed Rotating Disks," ASME *Journal of Basic Engineering,* Vol. 82, pp. 217–232.

Daily, J. W., and Nece, R. E., 1960b, "Roughness Effects on Frictional Resistance of Enclosed Rotating Disks," ASME *Journal of Basic Engineering,* Vol. 82, pp. 553–562.

Egli, A., 1935, "The Leakage of Steam Through Labyrinth Glands," *Trans. ASME,* Vol. 57, pp. 115–122.

Kosuge, H., Ito, T., and Nakanishi, K., 1982, "A Consideration Concerning Stall and Surge Limitations Within Centrifugal Compressors," ASME *Journal of Engineering for Power,* Vol. 104, pp. 782–787.

Lieblein, S., 1959, "Loss and Stall Analysis of Compressor Cascades," ASME *Journal of Basic Engineering,* Vol. 81, pp. 387–400.

Moussa, Z. M., 1978, "Impeller Casing Clearance Gap Flow Prediction Program," Carrier Corp. Technical Report 9-1030-05, No. 9 (proprietary).

Schlichting, H., 1979, *Boundary Layer Theory,* 7th ed., McGraw-Hill, New York, Chap. 20.

Weber, C. R., and Koronowski, M. E., 1986, "Meanline Performance Prediction of Volutes in Centrifugal Compressors," ASME Paper No. 86-GT-216.

Whitfield, A., and Baines, N. C., 1990, *Design of Radial Turbomachines,* Longman Scientific and Technical, Essex, United Kingdom.

Wiesner, F. J., 1967, "A Review of Slip Factors for Centrifugal Impellers," ASME *Journal of Engineering for Power,* Vol. 89, pp. 558–572.

APPENDIX

Clearance Gap Flows

Leakage, windage, and disk friction effects all require models of the clearance gap flows. This includes the disk/housing gap for the disk side and the shroud side for covered impellers, and the blade/housing clearance gap for open impellers. The flow in the disk/housing gap is modeled as a forced vortex:

$$\frac{\partial P}{\partial r} = K^2\omega^2\rho r \tag{34}$$

where $K = C_u/(\omega r)$ is assumed constant in the gap. An internal flow analysis for clearance gap flows (Moussa, 1978) was used to develop empirical relations for K, including the effects of seal leakage. Leakage was found to be quite significant due to the influx of angular momentum into the gap. In the absence of seal leakage, the data of Daily and Nece (1960a) suggest the following empirical equation:

$$K_0 = 0.46/(1 + 2s/d) \tag{35}$$

When leakage flow enters the gap with a swirl parameter K_F, the value of K in the gap is given by

$$K = K_0 + C_q(1.75K_F - 0.316)r_2/s$$

$$C_q = \frac{\dot{m}_L(\rho r_2 U_2/\mu)^{1/5}}{2\pi\rho r_2^2 U_2} \tag{36}$$

Typically, seal leakage from the tip employs $K_F = C_{u2}/U_2$ while leakage toward the tip uses $K_F = 0$. The validity of these approximations has been reasonably well established by comparing predicted and measured clearance gap radial static pressure profiles for select compressor stages. The resulting pressure distributions are used for predicting the seal leakage and for impeller thrust force calculations. Seal leakage is computed by the method of Egli (1935), although any other suitable formulation

could be substituted. Windage and disk friction is calculated with the Daily and Nece (1960a, 1960b) model with a correction for the clearance gap leakage flow. If the Daily and Nece torque coefficient is denoted as C_{M0}, the corrected value is given by

$$C_M = \frac{C_{M0}(1 - K)^2}{(1 - K_0)^2} \tag{37}$$

Equation (37) is somewhat intuitive, but has proven to yield very accurate work input predictions for ultralow flow coefficient stages (e.g., Compressor A) where leakage, windage, and disk friction play a very dominant roll. The torque coefficient is computed for each side of the disk and the disk and cover side values adjusted by

$$C_{MD} = 0.8C_M$$

$$C_{MC} = 0.8C_M \frac{L[1 - (d_{1s}/d_2)^5]}{r_2 - r_1} \tag{38}$$

where the constant 0.8 is an "experience" factor selected from correlation with numerous experimental stage work input curves. Since the Daily and Nece C_M refers to both sides of the disk, the factor of 0.8 actually imposes a torque coefficient about 60 percent higher than the Daily and Nece ideal disk flow correlation. Note that C_{MS} includes a correction for the different surface area (relative to a flat disk) for the impeller cover.

For the blade/housing clearance gap of open impellers, the velocity of the leakage flow through the clearance gap is given by

$$U_{CL} = 0.816\sqrt{2\Delta P_{CL}/\rho_2} \tag{39}$$

where the constant throttling coefficient of 0.816 was estimated by assuming an abrupt contraction followed by an abrupt expansion as the flow passes through the gap. The average pressure difference across the gap is estimated from the change in fluid angular momentum through the impeller:

$$\Delta P_{CL} = \frac{\dot{m}(r_2C_{u2} - r_1C_{u1})}{z\bar{r}\bar{b}L}$$

$$\bar{r} = (r_1 + r_2)/2$$

$$\bar{b} = (b_1 + b_2)/2 \tag{40}$$

Then the leakage flow is computed from

$$\dot{m}_{CL} = \rho z s L U_{CL} \tag{41}$$